

Fingering instability in adhesion fronts

M. L'Estimé¹, L. Duchemin¹, É. Reyssat¹ and J. Bico^{1,†}

¹Laboratoire de Physique et Mécanique des Milieux Hétérogènes (PMMH), CNRS, ESPCI Paris, Université PSL, Sorbonne Université, Université de Paris, Paris, France

(Received 14 May 2022; revised 4 August 2022; accepted 6 September 2022)

The adhesion of two surfaces relies on the propagation of an adhesion front. What is the dynamics of the front when both surfaces are coated with a thin layer of viscous liquid? Standard criteria from fingering instabilities would predict a stable front since viscous fluid pushes away air of low viscosity. Surprisingly, the front propagation may be unstable and generally leads to growing fingers. We demonstrate with model experiments where the two adhering surfaces are slightly tilted by an angle α that the origin of this interfacial instability relies on feeding the front from the surrounding thin film. We show experimentally that the typical wavelength of the instability is mainly dictated by the thickness of the oil layers h . In this wedge geometry, the propagation dynamics is found to follow a $t^{1/2}$ dependence and to saturate for an extension length of the order of h/α .

Key words: fingering instability, thin films

1. Introduction

Adhesion processes are key in numerous engineering and biological situations. The quality of adhesion is generally characterized through the separation of adjacent surfaces linked by a layer of bonding material. Such probe tack tests enable one to extract the rate-dependent work of adhesion (Creton & Ciccotti 2016). The separation process often involves instabilities when the adhesive layer is pulled apart, such as cavitation bubbles (Chiche, Dollhofer & Creton 2005) or viscous fingering patterns (Roy & Tarafdar 1996; Nase, Lindner & Creton 2008). Viscous fingering has been well documented since the seminal works from Saffman & Taylor (Saffman & Taylor 1958; McCloud & Maher 1995). This instability occurs when a viscous fluid is pushed away by a fluid of lower viscosity in a confined environment such as porous media or parallel plates (Hele-Shaw cell). The morphology of such patterns relies on confinement geometry (Rauseo, Barnes & Maher 1987; Al-Housseiny, Tsai & Stone 2012), fluid rheology (Bonn & Meunier 1997; Lindner, Coussot & Bonn 2000; Divoux *et al.* 2020) or surface anisotropy (Ben-Jacob *et al.* 1985). A closely related phenomenon is known as the printer's instability, which consists in the formation of ribbing patterns at the exit of the thin gap between two contra-rotating

† Email address for correspondence: jose.bico@espci.fr

cylinders coated with a thin liquid film (Pearson 1960; Pitts & Greiller 1961; Rabaud, Couder & Michalland 1991; Rabaud 1994). Analogous instabilities are also observed when plates separated by a layer of soft elastic material are pulled apart (Adda-Bedia & Mahadevan 2006; Biggins *et al.* 2013). In contrast, the dynamics of formation of adhesive contact has been overlooked. In a series of pioneering observations Zeng *et al.* (2006, 2007a,b) report the emergence of original fingering patterns during the contact of two spheres coated with a viscous polymer film. However, no quantitative prediction and measure of the fingers' size was provided. In the past decades, different studies have nevertheless been dedicated to the static pattern exhibited by a thin elastic film joining two solid surfaces (Ghatak *et al.* 2000; Mönch & Herminghaus 2001; Ghatak & Chaudhury 2003; Davis-Purcell *et al.* 2018). As we shall discuss later, the propagation of such fronts may be limited by the amount of fluid available in the thin films. This feature shares some similarity to diffusion-limited combustion fronts which also develop fingering patterns (Zik, Olami & Moses 1998; Zik & Moses 1999).

In the present paper, we focus on an experiment where two glass plates coated with a thin layer of viscous liquid are brought in contact. Once contact has nucleated, an unstable front propagates. What sets the adhesion dynamics? What are the characteristic size and time scales involved in the transient pattern? We address these questions through model experiments and scaling law analysis. We first present the experimental set-up and typical patterns of the adhesion front, and propose a qualitative mechanism to explain the formation of fingers. We then describe the geometric features of the observed patterns. We finally discuss the characteristic sizes and time scales involved in the dynamics of the adhesion front.

2. Experimental set-up

2.1. Preliminary experiment: contact of two adhesive plates

We first conduct the preliminary experiment depicted in figure 1(a) (see supplementary movie 1 available at <https://doi.org/10.1017/jfm.2022.789>): two glass plates both covered with a thin film of silicone oil are brought into contact in a roughly parallel fashion. The fluid layers have a thickness $h \sim 100 \mu\text{m}$ and the oil viscosity is $\eta = 50 \text{ mPa s}$. When put into contact, the oil layers start bridging in random places and the boundaries of the merged regions progressively invade the whole domain. Figure 1(b) shows successive top views of the experiment. In this configuration, the set-up is lit from above and image contrast results from reflection: the areas where oil layers have merged appear dark, while clear regions correspond to the remaining air gap. Shortly after contact, the front destabilizes into oil fingers separated by air channels. As these fingers propagate, the apparent area of air reduces gradually, leaving trapped bubbles at the end of the experiment. In this uncontrolled set-up, the patterns appear disorganized, both in time and space. Although locally regular, the propagation direction of the fingers is random on a large scale. Moreover, the dynamics is unsteady: in this particular example, the adhesion front almost stops after 13 s, before suddenly restarting. Nevertheless, this preliminary experiment reveals a regular pattern formation at small scale. In order to study quantitatively this new fingering phenomenon, we propose a better controlled wedge geometry for which the space–time dynamics is regular at large scale.

2.2. Controlled experiment: adhesion front in a wedge

The controlled set-up (figure 2a) is composed of two glass plates of thickness 4 mm, length 20 cm and width 10 cm, forming a wedge of angle α . The plates are covered with a thin

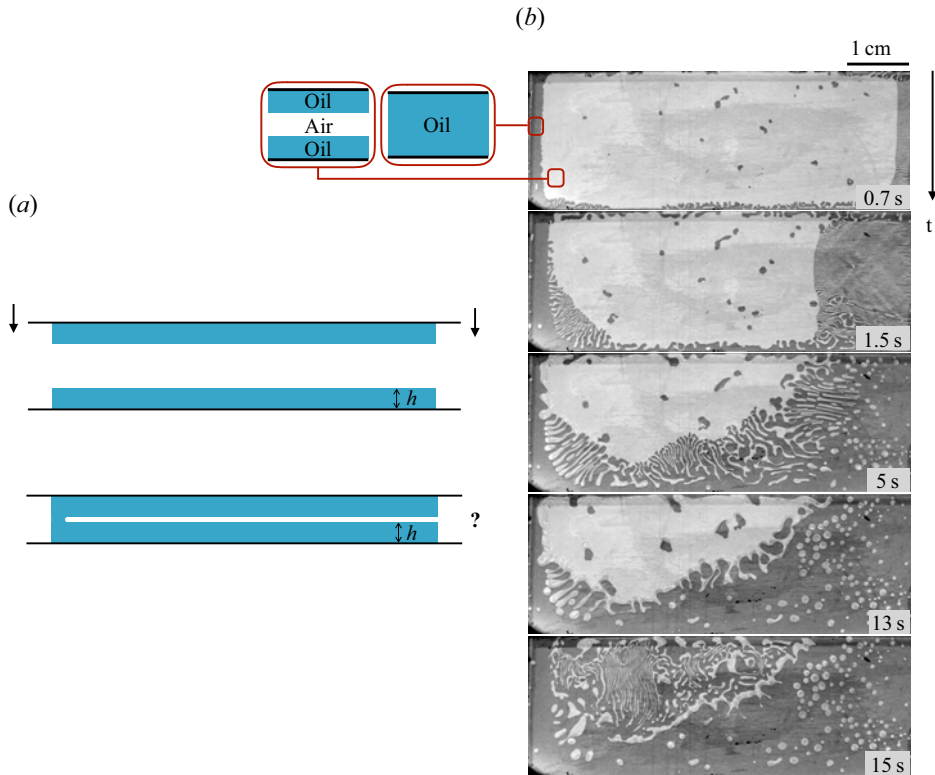


Figure 1. Preliminary experiment. (a) Side view: two glass plates covered with a thin layer of silicone oil of thickness h (in blue) are brought into contact. (b) Top view: areas where oil layers have merged appear dark, while clear regions correspond to the remaining air gap (see supplementary movie 1). The time since the first contact is indicated on the bottom right of the images.

layer of silicone oil of surface tension $\gamma \simeq 20 \text{ mN m}^{-1}$ and viscosity η ranging from 50 to 1000 mPa s. The coating is prepared by spreading a puddle of oil with a threaded roll along lateral adhesive tapes used as spacers. The uniformity of the coating is controlled with a confocal displacement sensor (CL-PT010 from Keyence). The thickness h of the oil layer is adjusted by varying the number of adhesive tapes separating the roll from the plate. In order to limit squeeze flows when the opposite plates are put in contact, a band of width 19 mm along the edge of the plates is not coated. This pristine region is obtained by placing a tape before coating and removing it prior to experiment. At the beginning of an experiment, the upper plate is placed over the lower one along one edge, while the plates are separated by a spacer at the opposite extremity (figure 2a).

Experimentally, the coating of the upper plate is prone to destabilization through Rayleigh–Taylor instability with a typical time scale $\tau_{RT} \sim 12\eta\gamma/h^3\rho^2g^2$ where ρ is the density of the fluid and g is the acceleration of gravity (Fermigier *et al.* 1992). In order to study the adhesion front dynamics without any interference from Rayleigh–Taylor instability, we chose our parameters such that the time scale for an experiment is much shorter than τ_{RT} . As a consequence, the maximum thickness of the coating films and the minimum viscosity were selected to be $h = 125 \mu\text{m}$ and $\eta = 50 \text{ mPa s}$, leading to $\tau_{RT} \sim 60 \text{ s}$, much larger than the instability time scale (of the order of a few seconds). Moreover, gravity drainage along the upper plate of length L occurs at even larger time

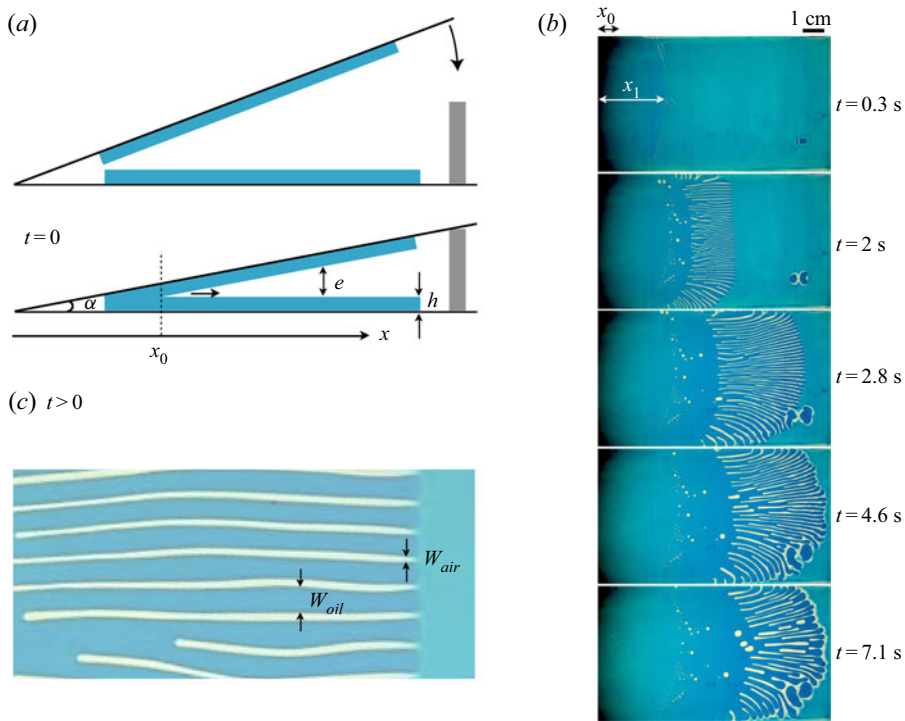


Figure 2. (a) Side view of the experimental set-up. Two glass plates covered with a thin layer of silicone oil of thickness h (in blue) form a sharp wedge of angle α adjusted with a spacer. An adhesion front immediately forms at a distance x_0 from the apex of the wedge. For $x > x_0$, the viscous films are separated by an air layer of thickness $e(x) \simeq \alpha(x - x_0)$ that has to be filled to achieve the adhesion. (b) Successive top views of an experiment conducted with dyed silicone oil of viscosity $\eta \simeq 50$ mPa s with layers of thickness $h \simeq 100$ μm (see also supplementary movie 2). The apex of the wedge of angle $\alpha \simeq 0.07^\circ$ is located along the left boundary of the pictures. The front quickly destabilizes into oil fingers separated by air channels. This pattern propagates towards the right and grows in length before slowly relaxing, eventually trapping small air bubbles between the plates. (c) Zoom on the destabilized front region, with the definitions of the widths W_{oil} and W_{air} of the oil fingers and air channels, respectively.

scale $\eta L / \rho g h^2 \sin \alpha \sim 5 h$. Within this range of thickness, we observed regular instability patterns for wedge angles typically lower than 0.3° , while the lowest angle that could be achieved with our set-up was of the order of 0.07° . For thick films and angles larger than 0.3° , the instability starts, but the fingers barely grow. In the following study, we focus on the regime of well-developed patterns for $\alpha \leq 0.25^\circ$.

Figure 2(b) shows successive top views of an experiment performed with silicone oil coloured with blue dye from Esprit Composite (see also supplementary movie 2). The plates are coated with films of initial thickness $h \simeq 100$ μm and viscosity $\eta \simeq 50$ mPa s. The apex of the wedge of angle $\alpha \simeq 0.07^\circ$ is located along the left boundary of the images. When the plates are brought into contact, the layers merge rapidly within a region of finite size x_0 from the apex. Although a stripe of width 19 mm has been carefully left pristine in the vicinity of the wedge to limit the overlap between the opposing layers, the position of the initial contact x_0 is prone to scatter due to unavoidable squeeze flow in this region. From there on, an air layer of thickness $e(x) \simeq \alpha(x - x_0)$ separates the facing layers, and the adhesion front moves forward from x_0 away from the apex. This front quickly destabilizes at a position x_1 from the apex, and leads to the formation of oil fingers

separated by air channels of widths W_{oil} and W_{air} respectively, as depicted in [figure 2\(c\)](#). In this configuration, the set-up is lit from underneath. The intensity of the oil colouring reflects the local oil thickness: deep blue corresponds to merged layers while light blue corresponds to the initial oil layers and white to air channels or bubbles.

As the tips of the fingers move faster than their rear, the length of the fingers increases. Later on, the tips of the fingers decelerate and eventually stop. In the meantime, the rear of the fingers keeps moving forward, reducing gradually the length of the fingers. At the end of the experiment the adhesion front recovers a smooth profile. During the retraction process, air channels tend to breakup into small bubbles, due to Rayleigh–Plateau instability, as often seen in microfluidic devices (Hashimoto *et al.* 2008; Guillot *et al.* 2009). These bubbles tend to slowly escape the most confined region of the wedge (Reyssat 2014).

3. Results and discussion

At first glance, this instability could seem similar to the classical Saffman–Taylor instability, as suggested by Zeng *et al.* (2006, 2007a). However, the standard criterion for viscous fingering would lead to a stable front since, here, viscous oil pushes away a low viscosity fluid (Saffman & Taylor 1958; Pelcé 2012). Moreover, in our configuration, the plates are not parallel as in the usual Hele–Shaw cell configuration. The effect of gradients of confinement in viscous fingering has recently been explored. When the displaced fluid does not wet the wall (as air in our situation), an opening gap tends to stabilize the front (Al-Housseiny *et al.* 2012). Classical printer’s instability also leads to ribbing patterns when a roller or spreader pushes a slab of viscous fluid at a fixed distance from a plane (Pearson 1960) or when a fluid is entrained between counter-rotating cylinders (Pitts & Greiller 1961; Rabaud 1994). However, this instability, as well as viscous fingering, is triggered by an imposed pressure gradient, which is not the case in our configuration. Beyond viscous fingering or printer’s instabilities, detergency effects in a gradient of confinement may also induce a capillary instability (Keiser *et al.* 2016). However, this last mechanism is not relevant to the current configuration as oil perfectly wets the wall and tends to remain trapped in the wedge. The formation of fingers is therefore driven by a mechanism distinct from the Saffman–Taylor or confinement gradient instabilities.

3.1. Qualitative mechanism

In order to bridge opposing surfaces, liquid must creep from ahead of the front to fill the air gap between the plates. If the front remained straight, its propagation would require the suction of fluid further ahead of the front. In this scenario, the thin coating films would soon become depleted ahead of the front, whose propagation would be severely hindered. Conversely, the formation of oil fingers leads to a partial bridging of the facing plates, which only requires local motion of the liquid from the films to the fingers. Indeed, we observe ([figure 2c](#)) that the regions between adjacent oil fingers appear clearer, indicating that the initial oil coating has been extracted laterally to form fingers. As the fingers propagate, the coating liquid separating them tends to drain out, leading to air channels. We do not observe any appreciable depletion of the coating films ahead of the tips when fingers move forward. However, a depleted zone quickly appears when the fingers cease to progress, as evidenced by the white line in the vicinity of the tips in the bottom image of [figure 2\(b\)](#).

This fingering mechanism is reminiscent of another instability observed by Zik *et al.* in the diffusion-limited combustion of sheets of paper confined in a horizontal Hele–Shaw

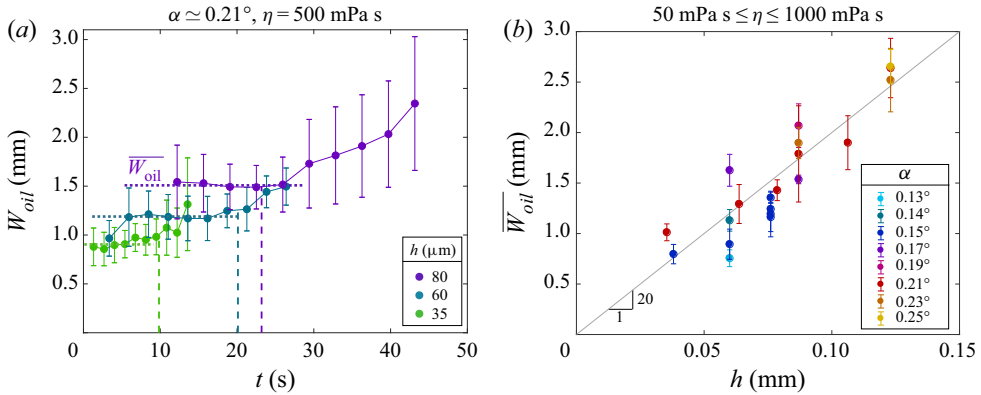


Figure 3. (a) Finger width W_{oil} averaged over several fingers as a function of time for experiments conducted with an angle $\alpha \simeq 0.21^\circ$, layers of thickness $h \simeq 35 \mu\text{m}$ (green), $60 \mu\text{m}$ (blue) and $80 \mu\text{m}$ (purple), of viscosity $\eta = 500 \text{ mPa s}$. The vertical dashed lines indicate the time at which the fingers have ceased to extend. As their width is nearly constant during the extension phase, the corresponding mean value \overline{W}_{oil} is computed for each experiment. (b) Mean finger width \overline{W}_{oil} during the extension phase as a function of the layer thickness h for experiments performed with angles α ranging from 0.13° to 0.25° , layers of thickness h ranging between 60 and $123 \mu\text{m}$ and viscosity $\eta = 50, 500$ or 1000 mPa s . The continuous line has a slope of 20 .

geometry (Zik *et al.* 1998; Zik & Moses 1999). As our adhesion front requires liquid to fill the air gap, the propagation of a combustion front relies on oxygen feeding. When the flux of oxygen is high enough, a straight front can propagate regularly, consuming oxygen ahead of it. However, reducing the flux prevents complete combustion from occurring and can induce the formation of ‘paper fingers’. Similarly to our mechanism, such fingers consume the oxygen available at the side of their tip and leave unconsumed ‘paper channels’ as they propagate.

3.2. Pattern geometry

As illustrated in figure 2(c) two main length scales describe the pattern morphology: the width W_{oil} of the oil fingers and the width W_{air} of the air channels.

3.2.1. Width of oil fingers

Figure 3(a) shows the width of the oil fingers W_{oil} as a function of time for experiments conducted with a wedge of angle $\alpha \simeq 0.21^\circ$ and layers of thickness $h \simeq 35, 60$ and $80 \mu\text{m}$. The vertical dashed lines indicate the time at which the fingers cease to extend. Beyond this point, the fingers begin to retract and their length decreases. As shown in figure 3(a), the width is approximately constant during the extension phase. It seems that the time-averaged width \overline{W}_{oil} is of the order of $20h$, as seen in figure 3(b). Once the fingers have reached their maximum position, their tip tends to retract and widen. Eventually fingers coalesce, leaving entrapped bubbles (figure 2b).

3.2.2. Width of air channels

Figure 4(a) shows the width of the air channels W_{air} as a function of time for an angle $\alpha \simeq 0.21^\circ$ and different layer thicknesses. For a given time and a given thickness of the coating layer, we observe that air channels are narrower than fingers. Contrary to the fingers, the width of air channels W_{air} increases over time. When W_{air} is plotted as a function of the

Fingering in adhesion fronts

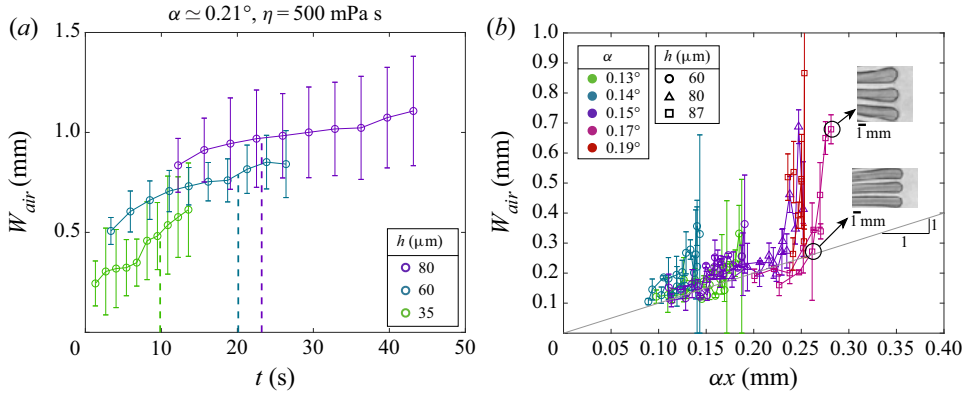


Figure 4. (a) Width of air channels averaged over several channels W_{air} as a function of time for experiments performed with $\alpha \simeq 0.21^\circ$ and layers of thickness $h \simeq 35 \mu\text{m}$ (green), $60 \mu\text{m}$ (blue) and $80 \mu\text{m}$ (purple). (b) Width of air channels displayed as a function of the spacing of the plates αx at the tip of the fingers. When the fingers stop their progression, the average width of the air channels tends to increase, as illustrated in the upper snapshot, which results in vertical spikes in the plot.

distance from the apex, we evidence that the width of the channels is set by the local distance between the plates

$$W_{air} \simeq \alpha x. \quad (3.1)$$

In other words, the section of air channels is basically circular in the stage when the front propagates. These channels eventually tend to widen after the front reaches its maximal position.

3.3. Speculative scenario

In this section, we suggest a preliminary explanation for the selection of the oil and air finger widths based on our experimental observation of the initial steps of the propagation of the front (figure 5a).

A front initiates at a finite distance x_0 from the apex of the wedge. In the very first stages of its progression, the front may remain smooth while a depleted region forms ahead of it (white stripe in transmitted light imaging). The front destabilizes at a position x_1 close to x_0 and organized lateral fingers progressively emerge. This pattern later evolves into more regular longitudinal fingers.

To interpret this sequence, we consider an ideal configuration where the liquid coatings initially form a perfect wedge (figure 5b, top). In this ideal geometry, the oil layers merge at a distance x_0 from the edge of the plates, where the distance between the glass plates is

$$x_0 = \frac{2h}{\alpha}. \quad (3.2)$$

From this position, a smooth front propagates, until the formation of fingers at a distance x_1 from the apex. This distance can be understood as the distance at which the propagation of a straight front is expected to stop. We would expect the front to stop when the size of the dimple becomes comparable to h . Assuming a circular dimple (figure 5b, bottom), the total liquid volume (per unit width) used to reach this configuration is of the order of h^2 . Moreover, a volume fills the initial air gap between x_0 and x_1 that is of the order of

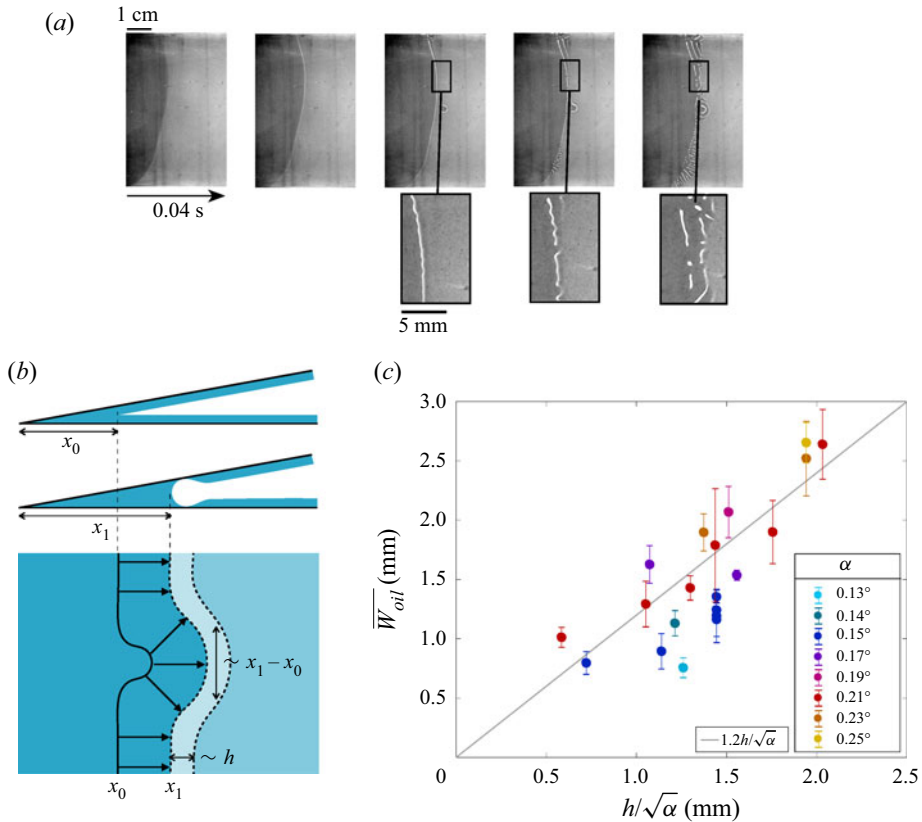


Figure 5. (a) Starting from an initial contact point of position x_0 , an initially smooth adhesion front propagates. As the front feeds from the liquid films coating the plates, these films are quickly depleted. White stripes are observed in the vicinity of the front beyond the position x_1 . (b) Top: ideal configuration where the liquid films form a perfect wedge at a distance x_0 from the apex of the cell. A straight front then propagates, feeding itself from the films up to a distance x_1 where the films neighbouring the front are depleted. Beyond x_1 , the front is expected to propagate through fingers feeding laterally and leaving air channels. Bottom: growth of a circular protrusion emerging as a perturbation, viewed from above. The maximum width of this protrusion is proportional to the displacement of the front $x_1 - x_0$. (c) Experimental values of \overline{W}_{oil} as a function of $h/\sqrt{\alpha}$.

$(x_1 - x_0)^2 \alpha / 2$, leading to a scaling

$$x_1 - x_0 \sim \frac{h}{\sqrt{\alpha}}. \tag{3.3}$$

With typical values $h = 100 \mu\text{m}$ and $\alpha = 0.2^\circ$, we obtain $x_1 - x_0 \sim 2 \text{ mm}$, which is much smaller than $x_0 \sim 60 \text{ mm}$. If a protrusion emerges spontaneously as a perturbation of the front profile and grows as a portion of a disk by feeding on the surrounding film, the maximum width of this protrusion should be also set by the distance $x_1 - x_0$. Beyond x_1 , the only possibility for the front to progress is to form oil fingers separated by air channels. We thus expect the width of the growing fingers to follow the same scaling

$$W_{oil} \sim \frac{h}{\sqrt{\alpha}}. \tag{3.4}$$

In figure 5(c), \overline{W}_{oil} is plotted as a function of $h/\sqrt{\alpha}$. Although data are still scattered as in figure 3(b), the slope is now of order 1, in agreement with (3.4). Probing this scenario

Fingering in adhesion fronts

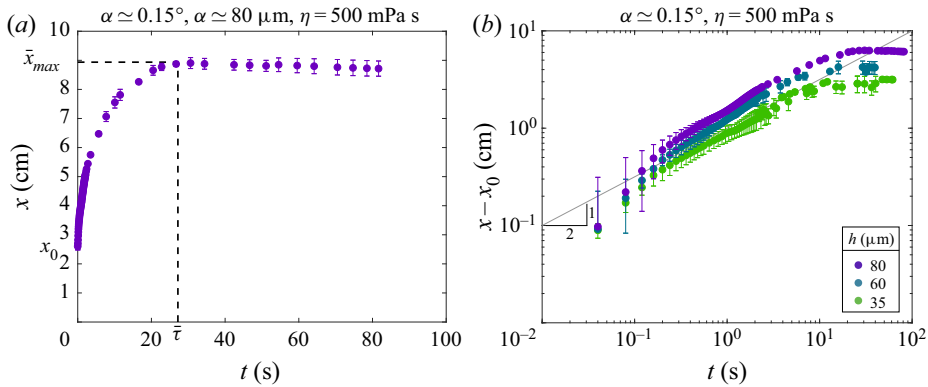


Figure 6. (a) Position x of the front as a function of time for an experiment performed with $\eta = 500$ mPa s, $\alpha \simeq 0.15^\circ$ and $h \simeq 80$ μm . The initial position of the front x_0 is geometrically set by the overlap of the coating layers when the wedge is closed at the beginning of the experiments. The fingers' tips reach their maximum position x_{max} at a characteristic time τ . (b) Relative position $x - x_0$ of the front as a function of time for experiments conducted with $\eta = 500$ mPa s, $\alpha \simeq 0.15^\circ$ and layers of thickness $h \simeq 35, 60$ and 80 μm . The continuous line in this log–log scale has a slope $1/2$.

more thoroughly would require experiments over a wider range of α (in particular smaller values), which is beyond our experimental capabilities. Numerical simulation could be an interesting tool to further explore this prediction.

3.4. Finger dynamics

We now focus on the dynamics of the fingers. The time evolution of the distance x from the edge of the plates to the tip of the fingers is plotted in figure 6(a) for an experiment conducted with $\eta = 500$ mPa s, $\alpha \simeq 0.21^\circ$ and $h \simeq 80$ μm . The fingers initially move relatively rapidly and progressively slow down until reaching a maximum position x_{max} at a characteristic rest time τ . The front starts at a finite distance x_0 from the apex that will be taken as a reference position for the front.

In an ideal configuration, x_0 should follow (3.2). Due to imperfections of the coating of the plates, the experimental value of x_0 tends to differ from this geometrical definition. Figure 6(b) compares the finger dynamics, relative to x_0 , for experiments performed with $\eta = 500$ mPa s, $\alpha \simeq 0.15^\circ$ and layers of thickness $h \simeq 35, 60$ and 80 μm . For each experiment, we observe that the relative position evolves as $t^{1/2}$ before saturation. Moreover, the relative position $x(t) - x_0$, the maximal position $x_{max} - x_0$ and the saturation time τ all increase with the layer thickness h .

We interpret these observations with simple scaling arguments. The capillary pressure $-\gamma/h$ in the fingers acts over a scale h in the thin film, leading to a typical pressure gradient $\nabla p \sim \gamma/h^2$. On the other hand, the viscous force density scales as $\eta v/h^2$, where v is the typical flow velocity of the liquid in the vicinity of the tip. Therefore, the balance of these two terms yields $v \sim \gamma/\eta$. The finger velocity $V_{tip} = d(x - x_0)/dt$ is then inferred from flux conservation. In the reference frame of the tip, as sketched in figure 7(a), the flux entering the tip, typically $hW_{oil}v$, compensates for the disappearing air gap $eW_{oil}V_{tip}$, leading to

$$hW_{oil}\frac{\gamma}{\eta} \sim eW_{oil}\frac{d(x - x_0)}{dt}. \quad (3.5)$$

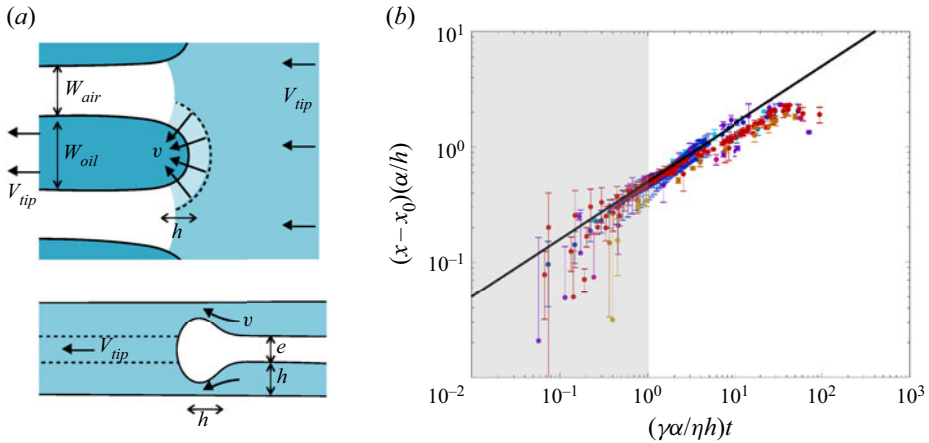


Figure 7. (a) Top and cross-sectional views of the cell as the liquid finger moves forward (in the reference frame of the finger). In the vicinity of the finger tip, the low pressure in the meniscus induces a flow from the feeding film to the finger characterized by a typical velocity $v \sim \gamma/\eta$. The velocity of the finger V_{tip} is deduced from flow conservation $hW_{oil}v \sim eW_{oil}V_{tip}$ leading to $x - x_0 \sim (\gamma ht/\eta\alpha)^{1/2}$. (b) Normalized position of the front as a function of normalized time for experiments performed with angles α ranging from 0.13° to 0.25° , layers of thickness h ranging from 60 to 125 μm and viscosities $\eta = 50, 500$ or 1000 mPa s. The black line corresponds to $(x - x_0)\alpha/h = 0.5(\gamma\alpha t/\eta h)^{1/2}$. The grey area indicates time scales smaller than $\eta h/\gamma\alpha$ (typically 1 s), which correspond to the setting phase of the experiment.

As the thickness of the air gap follows $e(x) = \alpha(x - x_0)$, (3.5) can be integrated

$$x - x_0 \sim \left(\frac{\gamma h}{\eta \alpha} t\right)^{1/2}. \quad (3.6)$$

Equation (3.6) is in good qualitative agreement with the data shown in figure 6(b). Figure 7(b) shows the dimensionless position of the fingers $(x - x_0)\alpha/h$ as a function of the dimensionless time $(\gamma\alpha/\eta h)t$, for various experiments performed with oils of viscosity ranging from 50 to 1000 mPa s, films thickness from 60 to 125 μm and wedge angle from 0.13° to 0.25° .

Although some scattering is observed, all experimental data tend to collapse onto the same master curve corresponding to (3.6). We interpret the scatter as a high sensitivity to initial conditions, in particular to the value selected for x_0 . The black curve in figure 7(b), in fair agreement with the experiments, corresponds to

$$(x - x_0)\frac{\alpha}{h} = 0.5 \left(\frac{\gamma\alpha}{\eta h} t\right)^{1/2}. \quad (3.7)$$

3.5. End of propagation

The evolution of the width of air channels with the distance from the apex $W_{air} \simeq \alpha x$ suggests that their cross-section is circular (figure 4). Air channels are formed by depleting the coating films along liquid fingers. Following the previous argument for the finger selection, the maximum volume available from the depletion of the films is of the order of h^2 per unit length. This area corresponds to the maximum area of the air channels. As a consequence, we expect the maximum value of W_{air} to be proportional to h . In other

Fingering in adhesion fronts

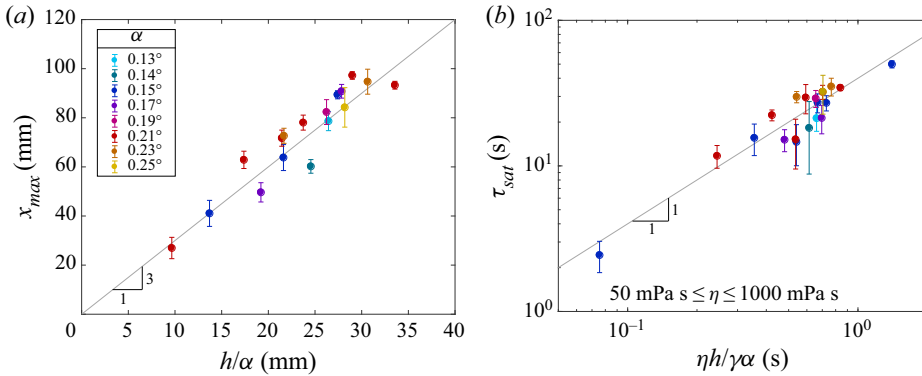


Figure 8. (a) Maximum relative position x_{max} as a function of the characteristic length h/α for experiments performed with angles α ranging from 0.13° to 0.25° , layers of thickness h ranging from 60 to $123 \mu\text{m}$ and viscosity $\eta = 50, 500$ or 1000 mPa s . The continuous line has a slope 3. (b) Saturation time measured experimentally τ_{sat} as a function of $\eta h/\gamma\alpha$. The continuous line corresponds to $\tau_{sat} = 40\eta h/\gamma\alpha$.

words, the propagation distance of the fingers x_{max} should follow the simple scaling

$$x_{max} \sim h/\alpha. \quad (3.8)$$

Experimental results obtained for angles α ranging from 0.13° to 0.25° and film thickness ranging from 60 to $125 \mu\text{m}$ indicate $x_{max} \simeq 3h/\alpha$, in good agreement with our prediction as shown in figure 8(a). Combining this expression with the approximated finger dynamics (3.7), and neglecting x_0 with respect to x_{max} , we can estimate the typical saturation time τ_{sat} required to reach the maximum position

$$\tau_{sat} \simeq 4x_{max}^2 \frac{\alpha^2 \eta h}{h^2 \gamma \alpha} \simeq 36 \frac{\eta h}{\gamma \alpha}. \quad (3.9)$$

The saturation time τ_{sat} measured experimentally is plotted as a function of $\eta h/\gamma\alpha$ in figure 8(b). The data collapse onto the black line corresponding to $\tau_{sat} = 40 \eta h/\gamma\alpha$, which confirms our description of the front dynamics.

4. Conclusion

We have explored experimentally an original fingering instability which occurs as two solid plates coated with thin viscous films of thickness h are brought into contact. More specifically, we explored a wedge configuration of angle α that leads to regular longitudinal fingers. The instability mechanism is distinct from classical viscous fingering and relies on feeding the air gap separating the facing surfaces from the liquid films. While a smooth front would deplete the liquid in its vicinity and stop at a typical distance $h/\sqrt{\alpha}$, fingers can propagate by absorbing the film laterally. We propose a simplified scenario where the constant width of the fingers is of the order of $W_{oil} \sim h/\sqrt{\alpha}$, in good agreement with our experimental data. Liquid fingers are separated by circular air channels whose diameter is dictated by the local spacing between the facing surfaces, $W_{air} \simeq \alpha x$. In this wedge configuration, the dynamics follows a diffusive scaling law $(\gamma h/\eta\alpha)^{1/2} t^{1/2}$ and stops at a characteristic length h/α for a typical time $\tau_{sat} \sim \eta h/\gamma\alpha$.

Many fundamental questions remain open. In particular, a rigorous stability analysis in this complex three-dimensional configuration is still missing. We also did not explore in detail the dynamics of the rear front nor the destabilization of air channels into individual

bubbles that are important for practical applications. Our experiment is finally also reminiscent of the merging of liquid films coating counter-rotating cylinders. Many works have been focused on the cusp profile of the interface (Joseph *et al.* 1991; Courrech du Pont & Eggers 2020) that precedes air entrainment as the rotation velocity of the cylinders is increased (Lorenceanu, Restagno & Quéré 2003). The limit of low rotation velocity has nevertheless received less attention. This regime might be close to our configuration and lead to a steady instability. We thus hope our experimental results will motivate further theoretical and numerical studies and experiments in similar configurations to address these challenging questions.

Supplementary movies. Supplementary movies are available at <https://doi.org/10.1017/jfm.2022.789>.

Acknowledgements. We thank P. Lalanne for his precious experimental help. J.B. is very grateful to T. Bohr and C. Clanet for fruitful discussions on preliminary experiments conducted in Copenhagen.

Declaration of interests. The authors report no conflict of interest.

Author ORCIDs.

✉ L. Duchemin <https://orcid.org/0000-0001-8179-4452>;

✉ É. Reyssat <https://orcid.org/0000-0003-3401-0111>;

✉ J. Bico <https://orcid.org/0000-0002-3872-1239>.

REFERENCES

- ADDA-BEDIA, M. & MAHADEVAN, L. 2006 Crack-front instability in a confined elastic film. *Proc. R. Soc. Lond. A* **462** (2075), 3233–3251.
- AL-HOUSSEINY, T.T., TSAI, P.A. & STONE, H.A. 2012 Control of interfacial instabilities using flow geometry. *Nat. Phys.* **8** (10), 747–750.
- BEN-JACOB, E., GODBEY, R., GOLDENFELD, N.D., KOPLIK, J., LEVINE, H., MUELLER, T. & SANDER, L.M. 1985 Experimental demonstration of the role of anisotropy in interfacial pattern formation. *Phys. Rev. Lett.* **55** (12), 1315–1318.
- BIGGINS, J.S., SAINTYVES, B., WEI, Z., BOUCHAUD, E. & MAHADEVAN, L. 2013 Digital instability of a confined elastic meniscus. *Proc. Natl Acad. Sci. USA* **110** (31), 12545–12548.
- BONN, D. & MEUNIER, J. 1997 Viscoelastic free-boundary problems: non-Newtonian viscosity vs normal stress effects. *Phys. Rev. Lett.* **79** (14), 2662–2665.
- CHICHE, A., DOLLHOFFER, J. & CRETON, C. 2005 Cavity growth in soft adhesives. *Eur. Phys. J. E* **17** (4), 389–401.
- COURRECH DU PONT, S. & EGGERS, J. 2020 Fluid interfaces with very sharp tips in viscous flow. *Proc. Natl Acad. Sci. USA* **117** (51), 32238–32243.
- CRETON, C. & CICCOTTI, M. 2016 Fracture and adhesion of soft materials: a review. *Rep. Prog. Phys.* **79** (4), 046601.
- DAVIS-PURCELL, B., SOULARD, P., SALEZ, T., RAPHAËL, E. & DALNOKI-VERESS, K. 2018 Adhesion-induced fingering instability in thin elastic films under strain. *Eur. Phys. J. E* **41** (3), 1–7.
- DIVOUX, T., SHUKLA, A., MARSIT, B., KALOGA, Y. & BISCHOFBERGER, I. 2020 Criterion for fingering instabilities in colloidal gels. *Phys. Rev. Lett.* **124** (24), 248006.
- FERMIGIER, M., LIMAT, L., WESFREID, J.E., BOUDINET, P. & QUILLIET, C. 1992 Two-dimensional patterns in Rayleigh–Taylor instability of a thin layer. *J. Fluid Mech.* **236**, 349–383.
- GHATAK, A. & CHAUDHURY, M.K. 2003 Adhesion-induced instability patterns in thin confined elastic film. *Langmuir* **19** (7), 2621–2631.
- GHATAK, A., CHAUDHURY, M.K., SHENOY, V. & SHARMA, A. 2000 Meniscus instability in a thin elastic film. *Phys. Rev. Lett.* **85** (20), 4329–4332.
- GUILLOT, P., AJDARI, A., GOYON, J., JOANICOT, M. & COLIN, A. 2009 Droplets and jets in microfluidic devices. *C. R. Chim.* **12** (1), 247–257.
- HASHIMOTO, M., GARSTECKI, P., STONE, H.A. & WHITESIDES, G.M. 2008 Interfacial instabilities in a microfluidic hele-shaw cell. *Soft Matt.* **4**, 1403–1413.
- JOSEPH, D.D., NELSON, J., RENARDY, M. & RENARDY, Y. 1991 Two-dimensional cusped interfaces. *J. Fluid Mech.* **223**, 383–409.

Fingering in adhesion fronts

- KEISER, L., HERBAUT, R., BICO, J. & REYSSAT, E. 2016 Washing wedges: capillary instability in a gradient of confinement. *J. Fluid Mech.* **790**, 619–633.
- LINDNER, A., COUSSOT, P. & BONN, D. 2000 Viscous fingering in a yield stress fluid. *Phys. Rev. Lett.* **85** (2), 314–317.
- LORENCEAU, E., RESTAGNO, F. & QUÉRÉ, D. 2003 Fracture of a viscous liquid. *Phys. Rev. Lett.* **90** (18), 184501.
- MCCLLOUD, K.V. & MAHER, J.V. 1995 Experimental perturbations to Saffman–Taylor flow. *Phys. Rep.* **260** (3), 139–185.
- MÖNCH, W. & HERMINGHAUS, S. 2001 Elastic instability of rubber films between solid bodies. *Europhys. Lett.* **53** (4), 525–531.
- NASE, J., LINDNER, A. & CRETON, C. 2008 Pattern formation during deformation of a confined viscoelastic layer: from a viscous liquid to a soft elastic solid. *Phys. Rev. Lett.* **101** (7), 074503.
- PEARSON, J.R.A. 1960 The instability of uniform viscous flow under rollers and spreaders. *J. Fluid Mech.* **7** (4), 481–500.
- PELCE, P. 2012 *Théorie des formes de croissance*. EDP Sciences.
- PITTS, E. & GREILLER, J. 1961 The flow of thin liquid films between rollers. *J. Fluid Mech.* **11** (1), 33–50.
- RABAUD, M. 1994 Dynamiques interfaciales dans l'instabilité de l'imprimeur. *Ann. Phys. France* **19**, 659–690.
- RABAUD, M., COUDER, Y. & MICHALLAND, S. 1991 Wavelength selection and transients in the one-dimensional array of cells of the printer's instability. *Eur. J. Mech. B* **10**, 253–260.
- RAUSEO, S.N., BARNES, P.D. Jr. & MAHER, J.V. 1987 Development of radial fingering patterns. *Phys. Rev. A* **35** (3), 1245–1251.
- REYSSAT, E. 2014 Drops and bubbles in wedges. *J. Fluid Mech.* **748**, 641–662.
- ROY, S. & TARAHDAR, S. 1996 Patterns in the variable hele-shaw cell for different viscosity ratios: similarity to river network geometry. *Phys. Rev. E* **54** (6), 6495–6499.
- SAFFMAN, P.G. & TAYLOR, G.I. 1958 The penetration of a fluid into a porous medium or Hele-Shaw cell containing a more viscous liquid. *Proc. R. Soc. Lond. A* **245** (1242), 312–329.
- ZENG, H., TIAN, Y., ZHAO, B., TIRRELL, M. & ISRAELACHVILI, J. 2007a Transient interfacial patterns and instabilities associated with liquid film adhesion and spreading. *Langmuir* **23** (11), 6126–6135.
- ZENG, H., TIAN, Y., ZHAO, B., TIRRELL, M. & ISRAELACHVILI, J. 2007b Transient surface patterns and instabilities at adhesive junctions of viscoelastic films. *Macromolecules* **40** (23), 8409–8422.
- ZENG, H., ZHAO, B., TIAN, Y., TIRRELL, M., LEAL, L.G. & ISRAELACHVILI, J.N. 2006 Transient surface patterns during adhesion and coalescence of thin liquid films. *Soft Matt.* **3** (1), 88–93.
- ZIK, O. & MOSES, E. 1999 Fingering instability in combustion: an extended view. *Phys. Rev. E* **60** (1), 518–531.
- ZIK, O., OLAMI, Z. & MOSES, E. 1998 Fingering instability in combustion. *Phys. Rev. Lett.* **81** (18), 3868–3871.